

Point-BERT: Pre-training 3D Point Cloud Transformers with Masked Point Modeling

Xumin Yu^{*1}, Lulu Tang^{*1,3}, Yongming Rao^{*1}, Tiejun Huang^{2,3}, Jie Zhou¹, Jiwen Lu^{†,1}

¹Department of Automation, Tsinghua University

²Department of Computer Science, Peking University

³Beijing Academy of Artificial Intelligence

Abstract

We present Point-BERT, a new paradigm for learning Transformers to generalize the concept of BERT [8] to 3D point cloud. Inspired by BERT, we devise a Masked Point Modeling (MPM) task to pre-train point cloud Transformers. Specifically, we first divide a point cloud into several local point patches, and a point cloud Tokenizer with a discrete Variational AutoEncoder (dVAE) is designed to generate discrete point tokens containing meaningful local information. Then, we randomly mask out some patches of input point clouds and feed them into the backbone Transformers. The pre-training objective is to recover the original point tokens at the masked locations under the supervision of point tokens obtained by the Tokenizer. Extensive experiments demonstrate that the proposed BERT-style pre-training strategy significantly improves the performance of standard point cloud Transformers. Equipped with our pre-training strategy, we show that a pure Transformer architecture attains 93.8% accuracy on ModelNet40 and 83.1% accuracy on the hardest setting of ScanObjectNN, surpassing carefully designed point cloud models with much fewer hand-made designs. We also demonstrate that the representations learned by Point-BERT transfer well to new tasks and domains, where our models largely advance the state-of-the-art of few-shot point cloud classification task. The code and pre-trained models are available at <https://github.com/lulutang0608/Point-BERT>.

1. Introduction

Compared to traditional hand-designed feature extraction methods, Convolutional Neural Networks (CNN) [21] is dependent on much less prior knowledge. Transformers [57] have pushed this trend further as a step towards no inductive bias with minimal man-made assumptions, such as translation equivalence or locality in CNNs. Recently,

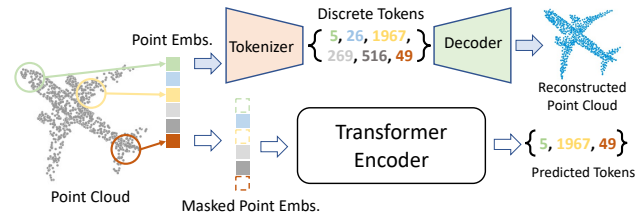


Figure 1. **Illustration of our main idea.** Point-BERT is designed for pre-training of standard point cloud Transformers. By training a dVAE via point cloud reconstruction, we can convert a point cloud into a sequence of discrete point tokens. Then we are able to pre-train the Transformers with a Mask Point Modeling (MPM) task by predicting the masked tokens.

the structural superiority and versatility of standard Transformers are proved in both language [3, 8, 19, 29, 42] and image tasks [2, 6, 9, 53, 63, 76], and the capability of diminishing the inductive biases is also justified by enabling more parameters, more data [9], and longer training schedules. Although Transformers produce astounding results in Natural Language Processing (NLP) and image processing, it is not well studied in the 3D community yet. Existing Transformer-based point cloud models [11, 72] bring in certain inevitable inductive biases from local feature aggregation [72] and neighbor embedding [11], making them deviate from the mainstream of standard Transformers. To this end, we aim to apply standard Transformers on point cloud directly with minimal inductive bias, as a stepping stone to a neat and unified model for 3D representation learning.

Apparently, the straightforward adoption of Transformers does not achieve satisfactory performance on point cloud tasks (see in Figure 5). This discouraging result is partially attributed to the limited annotated 3D data since pure Transformers with no inductive bias need massive training data. For example, ViT [9] uses ImageNet [21] (14M images) and JFT [50] (303M images) to train vision Transformers. In contrast, accurate annotated point clouds are relatively insufficient. Despite the 3D data acquisition

^{*}Equal contribution. [†]Corresponding author.

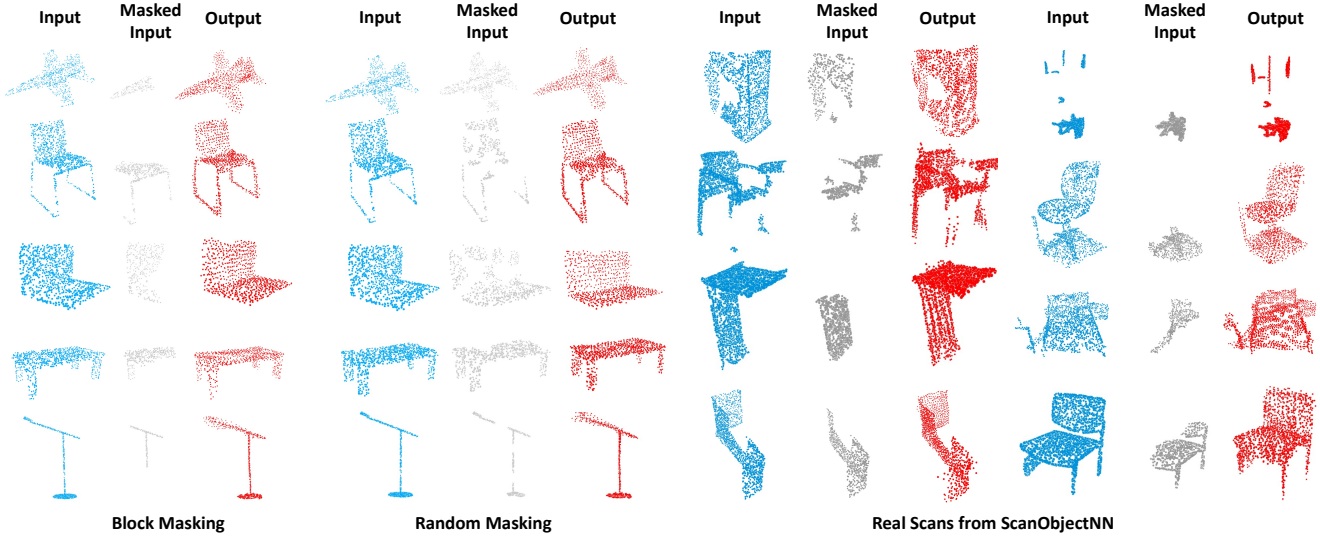


Figure 2. **Masked point clouds reconstruction using our Point-BERT model trained on ShapeNet.** We show the reconstruction results of synthetic objects from ShapeNet test set with block masking and random masking in the first two groups respectively. Our model also generalize well to unseen real scans from ScanObjectNN (the last two groups).

is getting easy with the recent proliferation of modern scanning devices, labeling point clouds is still time-consuming, error-prone, and even infeasible in some extreme real-world scenarios. The difficulty motivates a flux of research into learning from unlabelled 3D data. Self-supervised pre-training thereby becomes a viable technique to unleash the scalability and generalization of Transformers for 3D point cloud representation learning.

Among all the Transformer-based pre-training models, BERT [8] achieved state-of-the-art performance at its released time, setting a milestone in the NLP domain. Inspired by BERT [8], we seek to explore the BERT-style pre-training for 3D point cloud understanding. However, it is challenging to directly employ BERT on point clouds due to a lack of pre-existing vocabulary. In contrast, the language vocabulary has been well-defined (e.g., WordPiece in [8]) and off-the-shelf for model pre-training. In terms of point cloud Transformers, there is no pre-defined vocabulary for the point cloud. A naive idea is to treat every point as a ‘word’ and mimic BERT [8] to predict the coordinates of masked points. Such a point-wise regression task surges computational cost quadratically as the number of tokens increases. Moreover, a word in a sentence contains basic contextual semantic information, while a single point in a point cloud barely entails semantic meaning.

Nevertheless, a local patch partitioned from a holistic point cloud contains plentiful geometric information and can be treated as a component unit. *What if we build a vocabulary where different tokens represent different geometric patterns of the input units?* At this point, we can represent a point cloud as a sequence of such tokens. Now, we can favorably adopt BERT and its efficient implementa-

tions almost out of the box. We hypothesize that bridging this gap is a key to extending the successful Transformers and BERT to the 3D domain.

Driven by the above analysis, we present Point-BERT, a new scheme for learning point cloud Transformers. Two essential components are conceived:

- 1) Point Tokenization: A point cloud *Tokenizer* is devised via a dVAE-based [46] point cloud reconstruction, where a point cloud can be converted into discrete point tokens according to the learned vocabulary; We expect that the point tokens should imply the local geometric patterns, and the learned vocabulary should cover diverse geometric patterns, such that a sequence of such tokens can represent any point cloud (even never seen before).
- 2) Masked Point Modeling: A ‘masked point modeling’ (MPM) task is performed to pre-train Transformers, which masks a portion of input point cloud and learns to reconstruct the missing point tokens at the masked regions; We hope that our model enables reasoning the geometric relations among different patches of the point cloud, capturing meaningful geometric features for point cloud understanding.

Both two designs are implemented and justified in our experiments. We visualize the reconstruction results both on the synthetic (ShapeNet [5]) and real-world (ScanObjectNN [55]) datasets in Figure 2. We observe that our Point-BERT model correctly predicts the masked point tokens and infers diverse, holistic reconstructions through our dVAE decoder. The results suggest that the proposed model

has learned inherent and generic knowledge of 3D point clouds, i.e., geometric patterns or semantics. More significantly, our model is trained on ShapeNet, the masked point prediction results on ScanObjectNN reflect its superior performance on challenging scenarios with both unseen objects and domain gaps.

Our Point-BERT with a pure Transformer architecture and BERT-style pre-training technique achieves 93.8% accuracy on ModelNet40 and 83.1% accuracy on the complicated setting of ScanObjectNN, surpassing carefully designed point cloud models with much fewer human priors. We also show that the representations learned by Point-BERT transfer well to new tasks and domains, where our models largely advance the state-of-the-art of few-shot point cloud classification task. We hope a neat and unified Transformer architecture across images and point clouds could facilitate both domains since it enables joint modeling of 2D and 3D visual signals.

2. Related Work

Our point cloud pre-training model builds upon the work from the self-supervised learning, Transformers, and BERT-style pre-training, with 3D point cloud as an application. In this section, we try to give an overview of the recent advances in the aforementioned areas.

Self-supervised Learning (SSL). SSL is a type of unsupervised learning, where the supervision signals can be generated from the data itself [15]. The core idea of SSL is to define a pretext task, such as jigsaw puzzles [35], colorization [22], and optical-flow [33] in images. More recently, several studies suggested using SSL techniques for point cloud understanding [10, 14, 23, 36, 45, 47, 48, 51, 58, 62, 65]. Example 3D pretext tasks includes orientation estimation [38], deformation reconstruction [1], geometric structural cues [52] and spatial cues [34, 49]. Inspired by the jigsaw puzzles in images [35], [48] proposes to reconstruct point clouds from the randomly rearranged parts. A contrastive learning framework is proposed by DepthContrast [71] to learn representations from depth scans. More recently, OcCo [58] describes an encoder-decoder mechanism to reconstruct the occluded point clouds. Different from these studies, we attempt to explore a point cloud SSL model following the successful Transformers [57].

Transformers. Transformers [57] have recently become the dominant framework in NLP [3, 8, 19, 29, 42] due to its salient benefits, including massively parallel computing, long-distance characteristics, and minimal inductive bias. It has intrigued various vision tasks [12, 20], such as object classification [6, 9], detection [4, 76], segmentation [59, 73], pose estimation [17, 27], image generation [37], video processing [69, 75], and multimodality learning [41]. Nevertheless, its applications to 3D point cloud

remain limited. Some preliminary explorations have been implemented [11, 67, 72]. For instance, [72] applies the vectorized self-attention mechanism to construct a point Transformer layer for 3D point cloud learning. As a parallel work to [72], [11] uses a more typical Transformer architecture to learn point clouds, including a position encoding, an offset attention module, and a neighbor embedding. Nevertheless, prior efforts for Transformer-based point cloud models more or less involve some inductive biases, making them out of the line with standard Transformers. In this work, we seek to continue the success of standard Transformers and extend it to 3D point cloud learning, with minimal inductive bias.

BERT-style Pre-training. The main architecture of BERT [8] is built upon a multi-layer Transformer encoder, which is first designed to pre-train bidirectional representations from the unlabeled text in a self-supervised scheme. The primary ingredient that helps BERT stand out and achieve impressive performance is the pretext of Masked Language Modeling (MLM), which first randomly masks and then recovers a sequence of input tokens. The MLM strategy has also inspired a lot of pre-training tasks [2, 7, 19, 29, 54]. Take BEiT [2] for example, it first tokenizes the input image into discrete visual tokens. After that, it randomly masks some image patches and feeds the corrupted images into the Transformer backbone. The model is trained to recover the visual tokens of the masked patches. More recently, MAE [13] presents a masked autoencoder strategy for image representation learning. It first masks random patches of the input image and then encourages the model to reconstruct those missing pixels. Our work is greatly inspired by BEiT [2], which encodes the image into discrete visual tokens so that a Transformer backbone can be directly applied to these visual tokens. However, it is more challenging to acquire tokens for point clouds due to the unstructured nature of point clouds, which subsequently hinders the straightforward use of BERT on point clouds.

3. Point-BERT

The overall objective of this work is to extend the BERT-style pre-training strategy to point cloud Transformers. To achieve this goal, we first learn a *Tokenizer* to obtain discrete point tokens for each input point cloud. Mimicking the ‘MLM’ strategy in BERT [8], we devise a ‘masked point modeling’ (MPM) task to pre-train Transformers with the help of those discrete point tokens. The overall idea of our approach is illustrated in Figure 3.

3.1. Point Tokenization

In this section, we introduce how to tokenize a point cloud into a set of discrete tokens.

Point Embeddings. A naive approach treats per point as

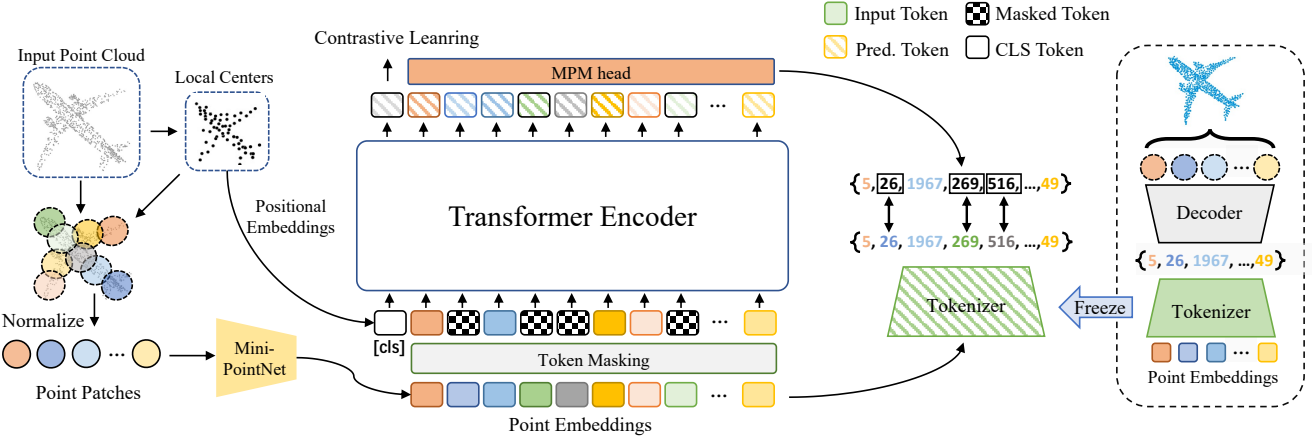


Figure 3. **The pipeline of Point-BERT.** We first partition the input point cloud into several point patches (sub-clouds). A mini-PointNet [39] is then used to obtain a sequence of point embeddings. Before pre-training, a *Tokenizer* is learned through dVAE-based point cloud reconstruction (as shown in the right part of the figure), where a point cloud can be converted into a sequence of discrete point tokens; During pre-training, we mask some portions of point embeddings and replace them with a mask token. The masked point embeddings are then fed into the Transformers. The model is trained to recover the original point tokens, under the supervision of point tokens obtained by the *Tokenizer*. We also add an auxiliary contrastive learning task to help the Transformers to capture high-level semantic knowledge.

one token. However, such a point-wise reconstruction task tends to unbearable computational cost due to the quadratic complexity of self-attention in Transformers. Inspired by the patch embedding strategy in Vision Transformers [9], we present a simple yet efficient implementation that groups each point cloud into several local patches (sub-clouds). Specifically, given an input point cloud $p \in \mathbb{R}^{N \times 3}$, we first sample g center points from the holistic point cloud p via farthest point sampling (FPS). The k-nearest neighbor (kNN) algorithm is then used to select the n nearest neighbor points for each center point, grouping g local patches (sub-clouds) $\{p_i\}_{i=1}^g$. We then make these local patches unbiased by subtracting their center coordinates, disentangling the structure patterns and spatial coordinates of the local patches. These unbiased sub-clouds can be treated as words in NLP or image patches in the vision domain. We further adopt a mini-PointNet [39] to project those sub-clouds into point embeddings. Following the practice of Transformers in NLP and 2D vision tasks, we represent a point cloud as a sequence of point embeddings $\{f_i\}_{i=1}^g$, which can be received as inputs to standard Transformers.

Point Tokenizer. Point *Tokenizer* takes point embeddings $\{f_i\}_{i=1}^g$ as the inputs and converts them into discrete point tokens. Specifically, the *Tokenizer* $\mathcal{Q}_\phi(z|f)$ maps point embeddings $\{f_i\}_{i=1}^g$ into discrete point tokens $\mathbf{z} = [z_1, z_2, \dots, z_g] \in \mathcal{V}$ ¹, where \mathcal{V} is the learned vocabulary with total length of N . In this step, the sub-clouds $\{p_i\}_{i=1}^g$ can be tokenized into point tokens $\{z_i\}_{i=1}^g$, relating to effective local geometric patterns. In our experiments,

¹Point tokens have two forms, discrete integer number and corresponding word embedding in \mathcal{V} , which are equivalent.

DGCNN [60] is employed as our *Tokenizer* network.

Point Cloud Reconstruction. The decoder $\mathcal{P}_\varphi(p|z)$ of dVAE receives point tokens $\{z_i\}_{i=1}^g$ as the inputs and learns to reconstruct the corresponding sub-clouds $\{p_i\}_{i=1}^g$. Since the local geometry structure is too complex to be represented by the limited N situations. We adopt a DGCNN [60] to build the relationship with neighboring point tokens, which can enhance the representation ability of discrete point tokens for diverse local structures. After that, a FoldingNet [65] is used to reconstruct the sub-clouds.

The overall reconstruction objective can be written as $\mathbb{E}_{z \sim \mathcal{Q}_\phi(z|p)} [\log \mathcal{P}_\varphi(p|z)]$, and the reconstruction procedure can be viewed as maximizing the evidence lower bound (ELB) of the log-likelihood $\mathcal{P}_\theta(p|\tilde{p})$ [43]:

$$\sum_{(p_i, \tilde{p}_i) \in \mathcal{D}} \log \mathcal{P}_\theta(p_i|\tilde{p}_i) \geq \sum_{(p_i, \tilde{p}_i) \in \mathcal{D}} (\mathbb{E}_{z_i \sim \mathcal{Q}_\phi(z|p_i)} [\log \mathcal{P}_\varphi(p_i|z_i)]) - D_{\text{KL}}[\mathcal{Q}_\phi(z|p_i), \mathcal{P}_\varphi(z|\tilde{p}_i)], \quad (1)$$

where p denotes the original point cloud, \tilde{p} denotes the reconstructed point cloud. Since the latent point tokens are discrete, we cannot apply the reparameterization gradient to train the dVAE. Following [43], we use the Gumbel-softmax relaxation [18] and a uniform prior during dVAE training. We refer to the supplementary for details about dVAE architecture and its implementation on point cloud reconstruction.

3.2. Transformer Backbone

We adopt the standard Transformers [57] in our experiments, consisting of multi-headed self-attention layers and FFN blocks. For each input point cloud, we first divide

it into g local patches with $\{c_i\}_{i=1}^g$ as the center points. Those local patches are then projected into point embeddings $\{f_i\}_{i=1}^g$ via a mini-PointNet [39], which consists of only MLP layers and the global maxpool operation. We further obtain the positional embeddings $\{pos_i\}$ of each patch by applying an MLP on its center point $\{c_i\}$. Formally, we define the input embeddings as $\{x_i\}_{i=1}^g$, which is the combination of point embeddings $\{f_i\}_{i=1}^g$ and positional embeddings $\{pos_i\}_{i=1}^g$. Then, we send the input embeddings $\{x_i\}_{i=1}^g$ into the backbone Transformer. Following [8], we append a class token $\mathbf{E}[s]$ to the input sequences. Thus, the input sequence of Transformer can be expressed as $H^0 = \{\mathbf{E}[s], x_1, x_2, \dots, x_g\}$. There are L layers of Transformer block in our model, and the output of the last layer $H^L = \{h_s^L, h_1^L, \dots, h_g^L\}$ represents the global feature, along with the encoded representation of the input sub-clouds.

3.3. Masked Point Modeling

Motivated by BERT [8] and BEiT [2], we extend the masked modeling strategy to point cloud learning and devise a masked point modeling (MPM) task to pre-train our Point-BERT.

Masked Sequence Generation. Different from the random masking used in BERT [8] and MAE [13], we adopt a block-wise masking strategy like [2]. Specifically, we first choose a center point c_i along with its sub-cloud p_i , and then find its m neighbor sub-clouds, forming a continuous local region. We mask out all local patches in this region to generate the masked point cloud. In practice, we directly apply such a block-wise masking strategy like [2] to the inputs of the Transformer. Formally, we mark the masked positions as $\mathcal{M} \in \{1, \dots, g\}^{\lfloor rg \rfloor}$, where r is the mask ratio. Next, we replace all the masked point embeddings with a same learnable pre-defined mask embeddings $\mathbf{E}[M]$ while keeping its positional embeddings unchanged. Finally, the corrupted input embeddings $\mathbf{X}^{\mathcal{M}} = \{x_i : i \notin \mathcal{M}\}_{i=1}^g \cup \{\mathbf{E}[M] + pos_i : i \in \mathcal{M}\}_{i=1}^g$ are fed into the Transformer encoder.

Pretext Task Definition. The goal of our MPM task is to enable the model to infer the geometric structure of missing parts based on the remaining ones. The pre-trained dVAE (see section 3.1) encodes each local patch into discrete point tokens, representing the geometric patterns. Thus, we can directly apply those informative tokens as our surrogate supervision signal to pre-train the Transformer.

Point Patch Mixing. Inspired by the CutMix [68, 70] technique, we additionally devise a neat mixed token prediction task as an auxiliary pretext task to increase the difficulty of pre-training in our Point-BERT, termed as ‘Point Patch Mixing’. Since the information of the absolute position of each sub-cloud has been excluded by normalization, we can

create new virtual samples by simply mixing two groups of sub-clouds without any cumbersome alignment techniques between different patches, such as optimal transport [70]. During pre-training, we also force the virtual sample to predict the corresponding tokens generated by the original sub-cloud to perform the MPM task. In our implementation, we generate the same number of virtual samples as the real ones to make the pre-training task more challenging, which is helpful to improve the training of Transformers with limited data as observed in [53].

Optimization Objective. The goal of MPM task is to recover the point tokens that are corresponding to the masked locations. The pre-training objective can be formalized as maximizing the log-likelihood of the correct point tokens z_i given the masked input embeddings $\mathbf{X}^{\mathcal{M}}$:

$$\max \sum_{\mathbf{X} \in D} \mathbb{E}_{\mathcal{M}} \left[\sum_{i \in \mathcal{M}} \log \mathcal{P}(z_i | \mathbf{X}^{\mathcal{M}}) \right]. \quad (2)$$

MPM task encourages the model to predict the masked geometric structure of the point clouds. Training the Transformer only with MPM task leads to an unsatisfactory understanding on high-level semantics of the point clouds, which is also pointed out by the recent work in 2D domain [74]. So we adopt the widely used contrastive learning method MoCo [14] as a tool to help the Transformers to better learn high-level semantics. With our point patch mixing technique, the optimization of contrastive loss encourages the model to pay attention to the high-level semantics of point clouds by making features of the virtual samples as closely as possible to the corresponding features from the original samples. Let q be the feature of a mixed sample that comes from two other samples, whose features are k_1^+ and k_2^+ ($\{k_i\}$ are extracted by the momentum feature encoder [14]). Assuming the mixing ratio is r , the contrastive loss can be written as:

$$\mathcal{L}_q = -r \log \frac{\exp(qk_1^+/\tau)}{\sum_{i=0}^K \exp(qk_i^+/\tau)} - (1-r) \log \frac{\exp(qk_2^+/\tau)}{\sum_{i=0}^K \exp(qk_i^+/\tau)}, \quad (3)$$

where τ is the temperature hyper-parameter and K is the size of memory bank. Coupling MPM objective and contrastive loss enables our Point-BERT to simultaneously capture the local geometric structures and high-level semantic patterns, which are crucial in point cloud representation learning.

4. Experiments

In this section, we first introduce the setups of our pre-training scheme. Then we evaluate the proposed model with various downstream tasks, including object classification, part segmentation, few-shot learning and transfer learning. We also conduct an ablation study for our Point-BERT.

Table 1. **Comparisons of Point-BERT with of state-of-the-art models on ModelNet40.** We report the classification accuracy (%) and the number of points in the input. [ST] and [T] represent the standard Transformers models and Transformer-based models with some special designs and more inductive biases, respectively.

Method	#point	Acc.
PointNet [39]	1k	89.2
PointNet++ [40]	1k	90.5
SO-Net [24]	1k	92.5
PointCNN [25]	1k	92.2
DGCNN [60]	1k	92.9
DensePoint [28]	1k	92.8
RSCNN [45]	1k	92.9
[T] PTC [11]	1k	93.2
[T] PointTransformer [72]	—	93.7
[ST] NPTC [11]	1k	91.0
[ST] Transformer	1k	91.4
[ST] Transformer + OcCo [58]	1k	92.1
[ST] Point-BERT	1k	93.2
[ST] Transformer	4k	91.2
[ST] Transformer + OcCo [58]	4k	92.2
[ST] Point-BERT	4k	93.4
[ST] Point-BERT	8k	93.8

4.1. Pre-training Setups

Data Setups. ShapeNet [5] is used as our pre-training dataset, which covers over 50,000 unique 3D models from 55 common object categories. We sample 1024 points from each 3D model and divide them into 64 point patches (sub-clouds). Each sub-cloud contains 32 points. A lightweight PointNet [39] containing two-layer MLPs is adopted to project each sub-cloud into 64 point embeddings, which are used as input both for dVAE and Transformer.

dVAE Setups. We use a four-layer DGCNN [60] to learn the inter-patch relationships, modeling the internal structures of input point clouds. During dVAE training, we set the vocabulary size N to 8192. Our decoder is also a DGCNN architecture followed by a FoldingNet [65]. It is worth noting that the performance of dVAE is susceptible to hyper-parameters, which makes that the configurations of image-based dVAE [44] cannot be directly used in our scenarios. The commonly used ℓ_1 -style Chamfer Distance loss is employed during the reconstruction procedure. Since the value of this ℓ_1 loss is numerically small, the weight of KLD loss in Eq.1 must be smaller than that in the image tasks. We set the weight of KLD loss to 0 in the first 10,000 steps and gradually increased to 0.1 in the following 100,000 steps. The learning rate is set to 0.0005 with a cosine learning schedule with 60,000 steps warming up. We decay the temperature in Gumble-softmax function from 1 to 0.0625 in 100,000 steps following [44]. We train dVAE

Table 2. **Few-shot classification results on ModelNet40.** We report the average accuracy (%) as well as the standard deviation over 10 independent experiments.

	5-way		10-way	
	10-shot	20-shot	10-shot	20-shot
DGCNN-rand [58]	31.6 ± 2.8	40.8 ± 4.6	19.9 ± 2.1	16.9 ± 1.5
DGCNN-OcCo [58]	90.6 ± 2.8	92.5 ± 1.9	82.9 ± 1.3	86.5 ± 2.2
DGCNN-rand*	91.8 ± 3.7	93.4 ± 3.2	86.3 ± 6.2	90.9 ± 5.1
DGCNN-OcCo*	91.9 ± 3.3	93.9 ± 3.1	86.4 ± 5.4	91.3 ± 4.6
Transformer-rand	87.8 ± 5.2	93.3 ± 4.3	84.6 ± 5.5	89.4 ± 6.3
Transformer-OcCo	94.0 ± 3.6	95.9 ± 2.3	89.4 ± 5.1	92.4 ± 4.6
Point-BERT	94.6 ± 3.1	96.3 ± 2.7	91.0 ± 5.4	92.7 ± 5.1

for a total of 150,000 steps with a batch size of 64.

MPM Setups. In our experiments, we set the depth for the Transformer to 12, the feature dimension to 384, and the number of heads to 6. The stochastic depth [16] with a 0.1 rate is applied in our transformer encoder. During MPM pre-training, we fix the weights of *Tokenizer* learned by dVAE. 25% ~ 45% input point embeddings are randomly masked out. The model is then trained to infer the expected point tokens at those masked locations. In terms of MoCo, we set the memory bank size to 16,384, temperature to 0.07, and weight momentum to 0.999. We employ an AdamW [31] optimizer, using an initial learning rate of 0.0005 and a weight decay of 0.05. The model is trained for 300 epochs with a batch size of 128.

4.2. Downstream Tasks

In this subsection, we report the experimental results on several downstream tasks. Besides the widely used benchmarks, including classification and segmentation, we also study the model’s capacity on few-shot learning and transfer learning.

Object Classification. We conduct classification experiments on ModelNet40 [61], the most popular 3D dataset for shape classification, which contains 12,311 synthesized CAD objects from 40 categories. We follow the previous works to split the dataset into 9843/2468 objects for training and validation. In the classification task, a two-layer MLP with a dropout of 0.5 is used as our classification head. We use AdamW with a weight decay of 0.05 and a learning rate of 0.0005 under a cosine schedule to optimize the model. The batch size is set to 32.

The results are presented in Table 1. We denote our baseline model as ‘Transformer’, which is trained on ModelNet40 with random initialization. Several Transformer-based models are illustrated, where [ST] represents a standard Transformer architecture, and [T] denotes the Transformer model with some special designs or inductive biases. Although we mainly focus on pre-training for standard Transformers in this work, our MPM pre-training strategy is also suitable for other Transformer-based point cloud

Table 3. **Part segmentation results on the ShapeNetPart dataset.** We report the mean IoU across all part categories $mIoU_C$ (%) and the mean IoU across all instance $mIoU_I$ (%) , as well as the IoU (%) for each categories.

Methods	$mIoU_C$	$mIoU_I$	aero	bag	cap	car	chair	earphone	guitar	knife	lamp	laptop	motor	mug	pistol	rocket	skateboard	table
PointNet [39]	80.39	83.7	83.4	78.7	82.5	74.9	89.6	73.0	91.5	85.9	80.8	95.3	65.2	93	81.2	57.9	72.8	80.6
PointNet++ [40]	81.85	85.1	82.4	79	87.7	77.3	90.8	71.8	91	85.9	83.7	95.3	71.6	94.1	81.3	58.7	76.4	82.6
DGCNN [60]	82.33	85.2	84	83.4	86.7	77.8	90.6	74.7	91.2	87.5	82.8	95.7	66.3	94.9	81.1	63.5	74.5	82.6
Transformer	83.42	85.1	82.9	85.4	87.7	78.8	90.5	80.8	91.1	87.7	85.3	95.6	73.9	94.9	83.5	61.2	74.9	80.6
Transformer-OcCo	83.42	85.1	83.3	85.2	88.3	79.9	90.7	74.1	91.9	87.6	84.7	95.4	75.5	94.4	84.1	63.1	75.7	80.8
Point-BERT	84.11	85.6	84.3	84.8	88.0	79.8	91.0	81.7	91.6	87.9	85.2	95.6	75.6	94.7	84.3	63.4	76.3	81.5

Table 4. **Classification results on the ScanObjectNN dataset.** We report the accuracy (%) of three different settings.

Methods	OBJ-BG	OBJ-ONLY	PB-T50-RS
PointNet [39]	73.3	79.2	68.0
SpiderCNN [64]	77.1	79.5	73.7
PointNet++ [40]	82.3	84.3	77.9
PointCNN [26]	86.1	85.5	78.5
DGCNN [60]	82.8	86.2	78.1
BGA-DGCNN [55]	—	—	79.7
BGA-PN++ [55]	—	—	80.2
Transformer	79.86	80.55	77.24
Transformer-OcCo	84.85	85.54	78.79
Point-BERT	87.43	88.12	83.07

models [11, 72]. Additionally, we compare with a recent pre-training strategy OcCo [58] as a strong baseline of our pre-training method. For fair comparisons, we follow the details illustrated in [58] and use the Transformer-based decoder PoinTr [67] to perform their pretext task. Combining our Transformer encoder and PoinTr’s decoder, we conduct the completion task on ShapeNet, following the idea of OcCo. We term this model as ‘Transformer+OcCo’.

We see pre-training Transformer with OcCo improves 0.7%/1.0% over the baseline using 1024/4096 inputs. In comparison, our Point-BERT brings 1.8%/2.2% gains over that of training from scratch. We also observe that adding more points will *not* significantly improve the Transformer model without pre-training while Point-BERT models can be consistently improved by increasing the number of points. When we increase the density of inputs (4096), our Point-BERT achieves significantly better performance (93.4%) than that with the baseline (91.2%) and OcCo (92.2%). Given more input points (8192), our method can be further boosted to 93.8% classification accuracy on ModelNet40.

Few-shot Learning. We follow previous work [49] to evaluate our model under the few-shot learning setting. A typical setting is “ K -way N -shot”, where K classes are first randomly selected, and then $(N+20)$ objects are sampled for each class [49]. The model is trained on $K \times N$ samples (support set), and evaluated on the remaining $20K$ samples (query set). We compare Point-BERT with OcCo

[58], which achieves state-of-the-art performance on this task. In our experiments, we test the performance under “5way 10shot”, “5way 20shot”, “10way 10shot” and “10way 20shot”. We conduct 10 independent experiments under each setting and report the average performance as well as the standard deviation over the 10 runs. We also reproduce DGCNN-rand and DGCNN-OcCo under the same condition for a fair comparison.

As shown in the Table 2, Point-BERT achieves the best performance in the few-shot learning task. It obtains an absolute improvement of 6.8%, 3.0%, 6.4%, 3.3% over the baseline and 0.6%, 0.4%, 1.6%, 0.3% over the OcCo-based method on the four settings. The strong results indicate that the model pre-trained by Point-BERT learns more generic knowledge that can be quickly transferred to new tasks with limited data.

Part Segmentation. Object part segmentation is a challenging task aiming to predict a more fine-grained class label for every point. We evaluate the effectiveness of Point-BERT on ShapeNetPart [66], which contains 16,881 models from 16 categories. Following PointNet [39], we sample 2048 points from each model and increase the group number g from 64 to 128 in the segmentation tasks. We design a segmentation head to propagate the group features to each point hierarchically. Specifically, features from 4th, 8th and the last layer of Transformer are selected, denoted as $\{H^4 = \{h_i^4\}_{i=1}^g, H^8 = \{h_i^8\}_{i=1}^g, H^{12} = \{h_i^{12}\}_{i=1}^g\}$. Then we downsample the origin point cloud to 512 and 256 points via FPS, phrased as $P^4 = \{p_i^4\}_{i=1}^{512}$ and $P^8 = \{p_i^8\}_{i=1}^{256}$. We follow PointNet++ [40] to perform feature propagation between H^4 and P^4 , H^8 and P^8 . Here, we can obtain the upsampled feature map \hat{H}^4 and \hat{H}^8 , which represent the features for the points in P^4 and P^8 . Then, we can propagate the feature from H^{12} to \hat{H}^4 and finally to every point.

Two types of mIoU are reported in Table 3. It is clear that our Point-BERT outperforms PointNet, PointNet++, and DGCNN. Moreover, Point-BERT improves 0.69% and 0.5% mIoU over vanilla Transformers, while OcCo fails to improve baseline performance in part segmentation task.

Transfer to Real-World Dataset. We evaluate the generalization ability of the learned representation by pre-training the model on ShapeNet and fine-tuning it on ScanOb-

Table 5. **Ablation study.** We investigate the effects of different designs and report the classification accuracy (%) after fine-tuning on ModelNet40. All models are trained with 1024 points.

Pretext tasks	MPM	Point Patch Mixing	Moco	Acc.
Model A				91.41
Model B	✓			92.58 ↑
Model C	✓	✓		92.91 ↑
Model D	✓	✓	✓	93.24 ↑
Augmentation	mask type	mask ratio	replace	Acc.
Model B	block mask	[0.25, 0.45]	No	92.58
Model B	block mask	[0.25, 0.45]	Yes	91.81 ↓
Model B	rand mask	[0.25, 0.45]	No	92.34 ↓
Model B	block mask	[0.55, 0.85]	No	92.52 ↓
Model D	block mask	[0.25, 0.45]	No	93.16
Model D	block mask	[0.25, 0.45]	Yes	92.58 ↓
Model D	rand mask	[0.25, 0.45]	No	92.91 ↓
Model D	block mask	[0.55, 0.85]	No	92.59 ↓

jectNN [55], which contains 2902 point clouds from 15 categories. It is a more challenging dataset sampled from real-world scans containing background and occlusions. We follow previous works to conduct experiments on three main variants: OBJ-BG, OBJ-ONLY, and PB-T50-RS. The experimental results are reported in Table 4. As we can see, Point-BERT improves the vanilla Transformers by about 7.57%, 7.57%, and 5.83% on three variants and outperforms OcCo consistently.

Comparing the classification results on ModelNet40 (Table 1) and ScanObjectNN (Table 2), we observe that DGCNN outperforms PointNet++ (+2.4%) on the ModelNet40. While the superiority is degraded on the real-world dataset ScanObjectNN. As for Point-BERT, it achieves SOTA performance on both datasets, which strongly confirms the effectiveness of our method.

4.3. Ablation Study

Pretext Task. We denote model A as our baseline, which is the Transformer training from scratch. Model B presents pre-training Transformer with MPM pretext task. Model C is trained with more samples coming from ‘point patch mixing’ technique. Model D (the proposed method) is trained under the setting of MPM, point patch mixing, and MoCo. As can be seen in the upper part of Table 5, Model B with only MPM improves the performance about 1.17% over the baseline Model A. By adopting point patch mixing strategy, Model C gets an improvement of 0.33%. With the help of MoCo [14], Model D further brings an improvement of 0.33%.

Masking Strategy. We visualize the point token prediction task in Figure 2. Our Transformer encoder can reasonably infer the point tokens of the missing patches. In practice, we reconstruct the local patches through the decoder of dVAE, based on the point tokens predicted by the Transformer en-

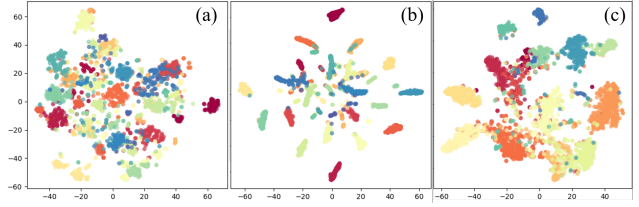


Figure 4. **Visualization of feature distributions.** We show the t-SNE visualization of feature vectors learned by Point-BERT (a) after pre-training, (b) after fine-tuning on ModelNet40, and (c) after fine-tuning on ScanObjectNN.

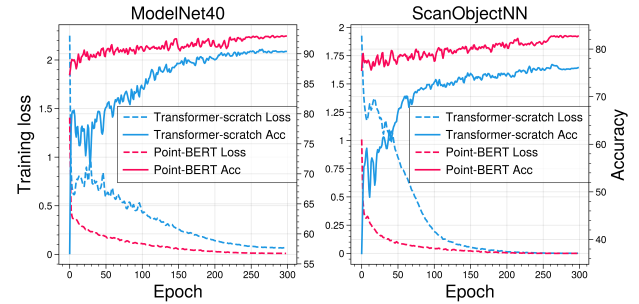


Figure 5. **Learning curve.** We compare the performance of Transformers training from scratch (blue) and pre-training with Point-BERT (red) in terms of training loss and validation accuracy on synthetic and real-world object classification datasets.

coder. Two masking strategies are explored: block-wise masking (block-mask) and random masking (rand-mask). The masking strategy determines the difficulty of the pretext task, influencing reconstruction quality and representations. We further investigate the effects of different masking strategies and provide the results in Table 5. We see that Model D with block-mask works better at the ratio of 25% ~ 45%. Unlike images, which can be split into regular non-overlapping patches, sub-clouds partitioned from the original point cloud often involve overlaps. Thus, rand-mask makes the task easier than block-mask, and further degrades the reconstruction performance. We also consider another type of augmentations: randomly replace some input embeddings with those from other samples. We find it unhelpful to our Point-BERT.

4.4. Visualization

We visualize the learned features of two datasets via t-SNE [56] in Figure 4. In figure (a) and (b), the visualized features are from our Point-BERT (a) before fine-tuning and (b) after fine-tuning on ModelNet40. As can be seen, features from different categories can be well separated by our method even before fine-tuning. It indicates that our pre-training strategy can effectively guide the Transformer to learn about object semantics without label supervision. We also visualize the feature maps on the PB-T50-RS of

ScanObjectNN in (c). We can see that separate clusters are formed for each category, indicating the transferability of learned representation to real-world scenarios. It further verifies the effectiveness of our Point-BERT that helps the Transformer to learn generic knowledge for 3D objects.

We also visualize the learning curves of our baseline Transformers and the proposed Point-BERT in Figure 5. As can be seen, pre-training with our Point-BERT significantly improves the performance of baseline Transformers both in accuracy and speed on both synthetic and real-world datasets.

5. Conclusion

We present a new paradigm for learning 3D point cloud Transformers through a BERT-style pre-training to learn both low-level structural information and high-level semantic feature of the point clouds. We observe a significant improvement for the Transformer on learning and generalization by comprehensive experiments on several 3D point cloud tasks, including object classification, object part segmentation, few-shot learning, and transfer learning. We show the potential of standard Transformers in 3D scenarios with appropriate pre-training strategy and look forward to further study on standard Transformers in the 3D domain.

6. Broader Impacts and Limitations

We develop a general paradigm for learning 3D point cloud Transformers in this paper. We do not foresee any negative ethical/societal impacts at this moment. Although the proposed method can effectively improve the performance of standard Transformers on point clouds, the entire ‘pre-training + fine-tuning’ procedure is rather time-consuming, like other Transformers pre-training methods [2, 8, 13]. Improving the efficiency of the training process will be an interesting future direction.

References

- [1] Idan Achituv, Haggai Maron, and Gal Chechik. Self-supervised learning for domain adaptation on point clouds. In *WACV*, 2021. 3
- [2] Hangbo Bao, Li Dong, and Furu Wei. Beit: Bert pre-training of image transformers. *arXiv preprint arXiv:2106.08254*, 2021. 1, 3, 5, 9
- [3] Tom B Brown, Benjamin Mann, Nick Ryder, Melanie Subbiah, Jared Kaplan, Prafulla Dhariwal, Arvind Neelakantan, Pranav Shyam, Girish Sastry, Amanda Askell, et al. Language models are few-shot learners. *arXiv preprint arXiv:2005.14165*, 2020. 1, 3
- [4] Nicolas Carion, Francisco Massa, Gabriel Synnaeve, Nicolas Usunier, Alexander Kirillov, and Sergey Zagoruyko. End-to-end object detection with transformers. In *ECCV*, 2020. 3
- [5] Angel X Chang, Thomas Funkhouser, Leonidas Guibas, Pat Hanrahan, Qixing Huang, Zimo Li, Silvio Savarese, Manolis Savva, Shuran Song, Hao Su, et al. Shapenet: An information-rich 3d model repository. *arXiv preprint arXiv:1512.03012*, 2015. 2, 6, 12
- [6] Mark Chen, Alec Radford, Rewon Child, Jeffrey Wu, Heewoo Jun, David Luan, and Ilya Sutskever. Generative pre-training from pixels. In *ICML*, 2020. 1, 3
- [7] Alexis Conneau and Guillaume Lample. Cross-lingual language model pretraining. *NeurIPS*, 2019. 3
- [8] Jacob Devlin, Ming-Wei Chang, Kenton Lee, and Kristina Toutanova. Bert: Pre-training of deep bidirectional transformers for language understanding. *arXiv preprint arXiv:1810.04805*, 2018. 1, 2, 3, 5, 9
- [9] Alexey Dosovitskiy, Lucas Beyer, Alexander Kolesnikov, Dirk Weissenborn, Xiaohua Zhai, Thomas Unterthiner, Mostafa Dehghani, Matthias Minderer, Georg Heigold, Sylvain Gelly, et al. An image is worth 16x16 words: Transformers for image recognition at scale. *arXiv preprint arXiv:2010.11929*, 2020. 1, 3, 4, 12
- [10] Benjamin Eckart, Wentao Yuan, Chao Liu, and Jan Kautz. Self-supervised learning on 3d point clouds by learning discrete generative models. In *CVPR*, 2021. 3
- [11] Meng-Hao Guo, Jun-Xiong Cai, Zheng-Ning Liu, Tai-Jiang Mu, Ralph R Martin, and Shi-Min Hu. Pct: Point cloud transformer. *Computational Visual Media*, 2021. 1, 3, 6, 7
- [12] Kai Han, Yunhe Wang, Hanting Chen, Xinghao Chen, Jianyu Guo, Zhenhua Liu, Yehui Tang, An Xiao, Chunjing Xu, Yixing Xu, et al. A survey on visual transformer. *arXiv preprint arXiv:2012.12556*, 2020. 3
- [13] Kaiming He, Xinlei Chen, Saining Xie, Yanghao Li, Piotr Dollár, and Ross Girshick. Masked autoencoders are scalable vision learners. *arXiv preprint arXiv:2111.06377*, 2021. 3, 5, 9
- [14] Kaiming He, Haoqi Fan, Yuxin Wu, Saining Xie, and Ross Girshick. Momentum contrast for unsupervised visual representation learning. In *CVPR*, 2020. 3, 5, 8
- [15] G Hinton, Y LeCunn, and Y Bengio. Aaai’2020 keynotes turing award winners event, 2020. 3
- [16] Gao Huang, Yu Sun, Zhuang Liu, Daniel Sedra, and Kilian Q Weinberger. Deep networks with stochastic depth. In *ECCV*, pages 646–661. Springer, 2016. 6
- [17] Lin Huang, Jianchao Tan, Ji Liu, and Junsong Yuan. Hand-transformer: non-autoregressive structured modeling for 3d hand pose estimation. In *ECCV*, 2020. 3
- [18] Eric Jang, Shixiang Gu, and Ben Poole. Categorical reparameterization with gumbel-softmax. *arXiv preprint arXiv:1611.01144*, 2016. 4
- [19] Mandar Joshi, Danqi Chen, Yinhan Liu, Daniel S Weld, Luke Zettlemoyer, and Omer Levy. Spanbert: Improving pre-training by representing and predicting spans. *TACL*, 2020. 1, 3
- [20] Salman Khan, Muzammal Naseer, Munawar Hayat, Syed Waqas Zamir, Fahad Shahbaz Khan, and Mubarak Shah. Transformers in vision: A survey. *arXiv preprint arXiv:2101.01169*, 2021. 3
- [21] Alex Krizhevsky, Ilya Sutskever, and Geoffrey E Hinton. Imagenet classification with deep convolutional neural networks. *NeurIPS*, 2012. 1

[22] Gustav Larsson, Michael Maire, and Gregory Shakhnarovich. Learning representations for automatic colorization. In *ECCV*, 2016. 3

[23] Jiaxin Li, Ben M Chen, and Gim Hee Lee. So-net: Self-organizing network for point cloud analysis. In *CVPR*, 2018. 3

[24] Jiaxin Li, Ben M Chen, and Gim Hee Lee. So-net: Self-organizing network for point cloud analysis. In *CVPR*, 2018. 6

[25] Yangyan Li, Rui Bu, Mingchao Sun, Wei Wu, Xinhua Di, and Baoquan Chen. Pointcnn: Convolution on x-transformed points. *NeurIPS*, 31, 2018. 6

[26] Yangyan Li, Rui Bu, Mingchao Sun, Wei Wu, Xinhua Di, and Baoquan Chen. Pointcnn: Convolution on x-transformed points. *NeurIPS*, 2018. 7

[27] Kevin Lin, Lijuan Wang, and Zicheng Liu. End-to-end human pose and mesh reconstruction with transformers. In *CVPR*, 2021. 3

[28] Yongcheng Liu, Bin Fan, Gaofeng Meng, Jiwen Lu, Shiming Xiang, and Chunhong Pan. Densepoint: Learning densely contextual representation for efficient point cloud processing. In *ICCV*, 2019. 6

[29] Yinhan Liu, Myle Ott, Naman Goyal, Jingfei Du, Mandar Joshi, Danqi Chen, Omer Levy, Mike Lewis, Luke Zettlemoyer, and Veselin Stoyanov. Roberta: A robustly optimized bert pretraining approach. *arXiv preprint arXiv:1907.11692*, 2019. 1, 3

[30] Ilya Loshchilov and Frank Hutter. Sgdr: Stochastic gradient descent with warm restarts. *arXiv preprint arXiv:1608.03983*, 2016. 12

[31] Ilya Loshchilov and Frank Hutter. Decoupled weight decay regularization. In *International Conference on Learning Representations*, 2018. 6

[32] Ilya Loshchilov and Frank Hutter. Fixing weight decay regularization in adam. 2018. 12

[33] Aravindh Mahendran, James Thewlis, and Andrea Vedaldi. Cross pixel optical-flow similarity for self-supervised learning. In *ACCV*, 2018. 3

[34] Benedikt Mersch, Xieyanli Chen, Jens Behley, and Cyrill Stachniss. Self-supervised point cloud prediction using 3d spatio-temporal convolutional networks. *arXiv preprint arXiv:2110.04076*, 2021. 3

[35] Mehdi Noroozi and Paolo Favaro. Unsupervised learning of visual representations by solving jigsaw puzzles. In *ECCV*, 2016. 3

[36] Aaron van den Oord, Yazhe Li, and Oriol Vinyals. Representation learning with contrastive predictive coding. *arXiv preprint arXiv:1807.03748*, 2018. 3

[37] Niki Parmar, Ashish Vaswani, Jakob Uszkoreit, Lukasz Kaiser, Noam Shazeer, Alexander Ku, and Dustin Tran. Image transformer. In *ICML*, 2018. 3

[38] Omid Poursaeed, Tianxing Jiang, Han Qiao, Nayun Xu, and Vladimir G Kim. Self-supervised learning of point clouds via orientation estimation. In *3DV*. IEEE, 2020. 3

[39] Charles R Qi, Hao Su, Kaichun Mo, and Leonidas J Guibas. Pointnet: Deep learning on point sets for 3d classification and segmentation. In *CVPR*, 2017. 4, 5, 6, 7

[40] Charles R Qi, Li Yi, Hao Su, and Leonidas J Guibas. Pointnet++ deep hierarchical feature learning on point sets in a metric space. In *NeurIPS*, 2017. 6, 7

[41] Alec Radford, Jong Wook Kim, Chris Hallacy, Aditya Ramesh, Gabriel Goh, Sandhini Agarwal, Girish Sastry, Amanda Askell, Pamela Mishkin, Jack Clark, et al. Learning transferable visual models from natural language supervision. *arXiv preprint arXiv:2103.00020*, 2021. 3

[42] Alec Radford, Jeffrey Wu, Rewon Child, David Luan, Dario Amodei, Ilya Sutskever, et al. Language models are unsupervised multitask learners. *OpenAI blog*, 2019. 1, 3

[43] Aditya Ramesh, Mikhail Pavlov, Gabriel Goh, Scott Gray, Chelsea Voss, Alec Radford, Mark Chen, and Ilya Sutskever. Zero-shot text-to-image generation. *arXiv preprint arXiv:2102.12092*, 2021. 4

[44] Aditya Ramesh, Mikhail Pavlov, Gabriel Goh, Scott Gray, Chelsea Voss, Alec Radford, Mark Chen, and Ilya Sutskever. Zero-shot text-to-image generation. *arXiv preprint arXiv:2102.12092*, 2021. 6, 12

[45] Yongming Rao, Jiwen Lu, and Jie Zhou. Global-local bidirectional reasoning for unsupervised representation learning of 3d point clouds. In *CVPR*, 2020. 3, 6

[46] Jason Tyler Rolfe. Discrete variational autoencoders. In *ICLR*, 2017. 2

[47] Aditya Sanghi. Info3d: Representation learning on 3d objects using mutual information maximization and contrastive learning. In *ECCV*, 2020. 3

[48] Jonathan Sauder and Bjarne Sievers. Self-supervised deep learning on point clouds by reconstructing space. *NeurIPS*, 2019. 3

[49] Charu Sharma and Manohar Kaul. Self-supervised few-shot learning on point clouds. *NeurIPS*, 2020. 3, 7

[50] Chen Sun, Abhinav Shrivastava, Saurabh Singh, and Abhinav Gupta. Revisiting unreasonable effectiveness of data in deep learning era. In *ICCV*, 2017. 1

[51] Chao Sun, Zhedong Zheng, Xiaohan Wang, Mingliang Xu, and Yi Yang. Point cloud pre-training by mixing and disentangling. *arXiv preprint arXiv:2109.00452*, 2021. 3

[52] Ali Thabet, Humam Alwassel, and Bernard Ghanem. Self-supervised learning of local features in 3d point clouds. In *CVPRW*, 2020. 3

[53] Hugo Touvron, Matthieu Cord, Matthijs Douze, Francisco Massa, Alexandre Sablayrolles, and Hervé Jégou. Training data-efficient image transformers & distillation through attention. In *ICML*, 2021. 1, 5, 13

[54] Trieu H Trinh, Minh-Thang Luong, and Quoc V Le. Selfie: Self-supervised pretraining for image embedding. *arXiv preprint arXiv:1906.02940*, 2019. 3

[55] Mikaela Angelina Uy, Quang-Hieu Pham, Binh-Son Hua, Thanh Nguyen, and Sai-Kit Yeung. Revisiting point cloud classification: A new benchmark dataset and classification model on real-world data. In *ICCV*, pages 1588–1597, 2019. 2, 7, 8

[56] Laurens Van der Maaten and Geoffrey Hinton. Visualizing data using t-sne. *Journal of machine learning research*, 2008. 8

[57] Ashish Vaswani, Noam Shazeer, Niki Parmar, Jakob Uszkoreit, Llion Jones, Aidan N Gomez, Łukasz Kaiser, and Illia Polosukhin. Attention is all you need. In *NeurIPS*, 2017. 1, 3, 4, 12, 13

[58] Hanchen Wang, Qi Liu, Xiangyu Yue, Joan Lasenby, and Matt J Kusner. Unsupervised point cloud pre-training via occlusion completion. In *ICCV*, 2021. 3, 6, 7

[59] Huiyu Wang, Yukun Zhu, Hartwig Adam, Alan Yuille, and Liang-Chieh Chen. Max-deeplab: End-to-end panoptic segmentation with mask transformers. In *CVPR*, 2021. 3

[60] Yue Wang, Yongbin Sun, Ziwei Liu, Sanjay E Sarma, Michael M Bronstein, and Justin M Solomon. Dynamic graph cnn for learning on point clouds. *TOG*, 2019. 4, 6, 7, 12, 14

[61] Zhirong Wu, Shuran Song, Aditya Khosla, Fisher Yu, Lin-guang Zhang, Xiaou Tang, and Jianxiong Xiao. 3d shapenets: A deep representation for volumetric shapes. In *CVPR*, 2015. 6

[62] Saining Xie, Jiatao Gu, Demi Guo, Charles R Qi, Leonidas Guibas, and Or Litany. Pointcontrast: Unsupervised pre-training for 3d point cloud understanding. In *ECCV*, 2020. 3

[63] Zhenda Xie, Yutong Lin, Zhuliang Yao, Zheng Zhang, Qi Dai, Yue Cao, and Han Hu. Self-supervised learning with swin transformers. *arXiv preprint arXiv:2105.04553*, 2021. 1

[64] Yifan Xu, Tianqi Fan, Mingye Xu, Long Zeng, and Yu Qiao. Spidercnn: Deep learning on point sets with parameterized convolutional filters. In *ECCV*, 2018. 7

[65] Yaoqing Yang, Chen Feng, Yiru Shen, and Dong Tian. Foldingnet: Point cloud auto-encoder via deep grid deformation. In *CVPR*, 2018. 3, 4, 6, 12

[66] Li Yi, Vladimir G Kim, Duygu Ceylan, I-Chao Shen, Mengyan Yan, Hao Su, Cewu Lu, Qixing Huang, Alla Sheffer, and Leonidas Guibas. A scalable active framework for region annotation in 3d shape collections. *ToG*, 35(6):1–12, 2016. 7

[67] Xumin Yu, Yongming Rao, Ziyi Wang, Zuyan Liu, Jiwen Lu, and Jie Zhou. Pointr: Diverse point cloud completion with geometry-aware transformers. In *ICCV*, 2021. 3, 7, 12

[68] Sangdoo Yun, Dongyoon Han, Seong Joon Oh, Sanghyuk Chun, Junsuk Choe, and Youngjoon Yoo. Cutmix: Regularization strategy to train strong classifiers with localizable features. In *ICCV*, 2019. 5

[69] Yanhong Zeng, Jianlong Fu, and Hongyang Chao. Learning joint spatial-temporal transformations for video inpainting. In *ECCV*, 2020. 3

[70] Jinlai Zhang, Lyujie Chen, Bo Ouyang, Binbin Liu, Jihong Zhu, Yujing Chen, Yanmei Meng, and Danfeng Wu. Pointcutmix: Regularization strategy for point cloud classification. *arXiv preprint arXiv:2101.01461*, 2021. 5

[71] Zaiwei Zhang, Rohit Girdhar, Armand Joulin, and Ishan Misra. Self-supervised pretraining of 3d features on any point-cloud. *arXiv preprint arXiv:2101.02691*, 2021. 3

[72] Hengshuang Zhao, Li Jiang, Jiaya Jia, Philip HS Torr, and Vladlen Koltun. Point transformer. In *ICCV*, 2021. 1, 3, 6, 7

[73] Sixiao Zheng, Jiachen Lu, Hengshuang Zhao, Xiatian Zhu, Zekun Luo, Yabiao Wang, Yanwei Fu, Jianfeng Feng, Tao Xiang, Philip HS Torr, et al. Rethinking semantic segmentation from a sequence-to-sequence perspective with transformers. In *CVPR*, 2021. 3

[74] Jinghao Zhou, Chen Wei, Huiyu Wang, Wei Shen, Ci-hang Xie, Alan Yuille, and Tao Kong. Ibot: Image bert pre-training with online tokenizer. *arXiv preprint arXiv:2111.07832*, 2021. 5

[75] Luowei Zhou, Yingbo Zhou, Jason J Corso, Richard Socher, and Caiming Xiong. End-to-end dense video captioning with masked transformer. In *CVPR*, 2018. 3

[76] Xizhou Zhu, Weijie Su, Lewei Lu, Bin Li, Xiaogang Wang, and Jifeng Dai. Deformable detr: Deformable transformers for end-to-end object detection. In *ICLR*, 2020. 1, 3

Appendix: Implementation Details

A. Discrete VAE

Architecture: Our dVAE consists of a tokenizer and a decoder. Specifically, the tokenizer contains a 4-layer DGCNN [60], and the decoder involves a 4-layer DGCNN followed by a FoldingNet [65]. The detailed network architecture of our dVAE is illustrated in Table 6, where C_{in} and C_{out} are the dimension of input and output features, C_{middle} is the dimension of the hidden layers. N_{out} is the number of point patches in each layer, and K is the number of neighbors in kNN operation. Additionally, `FoldingLayer` concatenates a 2D grids to the inputs and finally generates 3D point clouds.

Table 6. **Detailed architecture of our models.** C_{in}/C_{out} represents the dimension of input/output features, and N_{out} is the number of points in the query point cloud. K is the number of neighbors in kNN operation. C_{middle} is the dimension of the hidden layers for MLPs.

Module	Block	C_{in}	C_{out}	K	N_{out}	C_{middle}
dVAE Tokenizer	Linear	256	128			
	DGCNN	128	256	4	64	
	DGCNN	256	512	4	64	
	DGCNN	512	512	4	64	
	DGCNN	512	1024	4	64	
	Linear	2304	8192			
dVAE Decoder	Linear	256	128			
	DGCNN	128	256	4	64	
	DGCNN	256	512	4	64	
	DGCNN	512	512	4	64	
	DGCNN	512	1024	4	64	
	Linear	2304	256			
	MLP	256	48			1024
	FoldingLayer	256	3			1024
Classification Head	MLP	768	N_{cls}			256
Segmentation Head	MLP	387	384			384×4
	DGCNN	384	512	4	128	
	DGCNN	512	384	4	128	
	DGCNN	384	512	4	256	
	DGCNN	512	384	4	256	
	DGCNN	384	512	4	512	
	DGCNN	512	384	4	512	
	DGCNN	384	512	4	2048	
	DGCNN	512	384	4	2048	

Optimization: During the training phase, we consider reconstruction loss and distribution loss simultaneously. For reconstruction, we follow PoinTr [67] to supervise both coarse-grained prediction and fine-grained prediction with the ground-truth point cloud. The ℓ_1 -form Chamfer Distance is adopted, which is calculated as:

$$d_{CD}^{\ell_1}(\mathcal{P}, \mathcal{G}) = \frac{1}{|\mathcal{P}|} \sum_{p \in \mathcal{P}} \min_{g \in \mathcal{G}} \|p - g\| + \frac{1}{|\mathcal{G}|} \sum_{g \in \mathcal{G}} \min_{p \in \mathcal{P}} \|g - p\|, \quad (1)$$

where \mathcal{P} represents the prediction point set and \mathcal{G} represents the ground-truth point set. Except for the reconstruction

Table 7. **Experiment setting for training the dVAE.**

config	value
optimizer	AdamW [32]
learning rate	5e-4
weight decay	5e-4
learning rate schedule	cosine [30]
warmingup epochs	10
augmentation	RandSampling
batch size	64
number of points	1024
number of patches	64
patch size	32
training epochs	300
dataset	ShapeNet [5]

loss, we follow [44] to optimize the KL-divergence \mathcal{L}_{KL} between the predicted tokens’ distribution and a uniform prior. The final objective function is

$$\mathcal{L}_{dVAE} = d_{CD}^{\ell_1}(\mathcal{P}_{fine}, \mathcal{G}) + d_{CD}^{\ell_1}(\mathcal{P}_{coarse}, \mathcal{G}) + \alpha \mathcal{L}_{KL}. \quad (2)$$

Experiment Setting: We report the default setting for dVAE training in Table 7.

Hyper-parameters of dVAE: We set the size of the learnable vocabulary to 8192, and each ‘word’ in it is a 256-dim vector. The most important and sensitive hyper-parameters of dVAE are α for \mathcal{L}_{KL} and the temperature τ for Gumbel-softmax. We set α to 0 in the first 18 epochs (about 10,000 steps) and gradually increase to 0.1 in the following 180 epochs (about 100,000 steps) using a cosine schedule. As for τ , we follow [44] to decay it from 1 to 0.0625 using a cosine schedule in the first 180 epochs (about 100,000 steps).

B. Point-BERT

Architecture: We follow the standard Transformer [9] architecture in our experiments. It contains a stack of Transformer blocks [57], and each block consists of a multi-head self-attention layer and a FeedForward Network (FFN). In these two layers, LayerNorm (LN) is adopted.

Multi-head Attention: Multi-head attention mechanism enables the network to jointly consider information from different representation subspaces [57]. Specifically, given the input values V , keys K and queries Q , the multi-head attention is computed by:

$$\text{MultiHead}(Q, K, V) = W^o \text{Concat}(\text{head}_1, \dots, \text{head}_h), \quad (3)$$

where W^o is the weights of the last linear layer. The feature of each head can be obtained by:

$$\text{head}_i = \text{softmax}\left(\frac{QW_i^Q(KW_i^K)^T}{\sqrt{d_k}}\right)VW_i^V, \quad (4)$$

config	value
optimizer	AdamW
learning rate	5e-4
weight decay	5e-2
learning rate schedule	cosine
warmingup epochs	3
augmentation	ScaleAndTranslate
batch size	128
number of points	1024
number of patches	64
patch size	32
mask ratio	[0.25, 0.45]
mask type	rand mask
training epochs	300
dataset	ShapeNet

Table 8. Experiment setting for Point-BERT pre-training

config	value
optimizer	AdamW
learning rate	5e-4
weight decay	5e-2
learning rate schedule	cosine
warmingup epochs	10
augmentation	ScaleAndTranslate
batch size	32(C), 16(S)
number of points	1024(C), 2048 (S)
number of patches	64(C), 128(S)
patch size	32
training epochs	300

Table 9. Experiment setting for end-to-end finetuning. S represents segmentation task, C represents classification task.

where W_i^Q , W_i^K and W_i^V are the linear layers that project the inputs to different subspaces and d_k is the dimension of the input features.

Feed-forward network (FFN): Following [57], two linear layers with ReLU activations and dropout are adopted as the feed-forward network.

Point-BERT pre-training: We report the default setting for our experiments in Point-BERT pretraining in Table 8. The pre-training is conducted on ShapeNet.

End-to-end finetuning: We finetune our Point-BERT model follow the common practice of supervised models strictly. The default setting for end-to-end finetuning is in Table 9.

Hyper-parameters of Transformers: We set the number of blocks in the Transformer to 12. The number of heads in each multi-head self-attention layer is set to 6. The feature

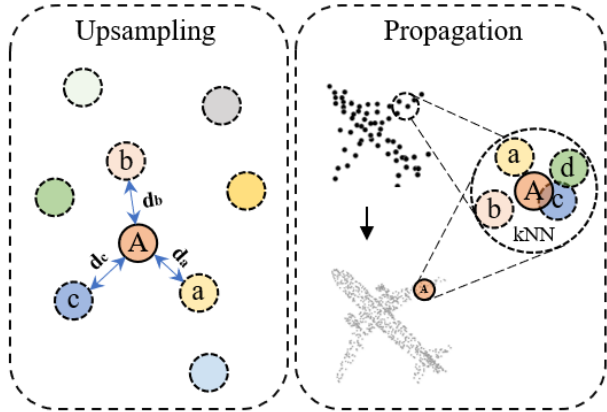


Figure 6. Two main operations of our segmentation head: 1) Upsampling: upsample the feature map for the sparse point cloud to the dense point cloud. 2) Propagation: propagate the feature hierarchically from deep layers to shallow layers for dense prediction.

dimension of the transformer layer is set to 384. We follow [53] to adopt the stochastic depth strategy with a drop rate of 0.1.

Classification Head: A two-layer MLP with dropout is applied as our classification head. In classification tasks, we first take the output feature of [CLS] token out, and max-pool the rest of nodes' features. These two features are then combined together and sent into the classification head. The detailed architecture of the classification head is shown in Table 6, where N_{cls} is the number of classes for a certain dataset.

Segmentation Head: There are no downsampling layers in the standard Transformers, making it challenging to perform dense prediction based on a single-resolution feature map. We adopt an upsampling-propagation strategy to solve this problem, consisting of two steps: 1) Geometry-based feature upsampling and 2) Hierarchical feature propagation.

We extract features from different layers of the Transformer, where features from shallow layers tend to capture low-level information, while features from deeper layers involve more high-level information. To upsample the feature maps to different resolutions, we first apply FPS to the origin point cloud and obtain point clouds at various resolutions. Then we upsample the feature maps from different layers to different resolutions accordingly. As shown in the left part of Figure 6, ‘A’ is a point from the dense point cloud, and ‘a’, ‘b’, ‘c’ are its nearest points in the sparser point cloud, with distance of d_a , d_b and d_c respectively. We obtain the point feature of ‘A’ based on the weighted addition of those features, which can be written as:

$$\mathcal{F}_A = \text{MLP}(\text{Concat}\left(\frac{\sum_{i \in [a,b,c]} \frac{1}{d_i} \mathcal{F}_i}{\sum_{i \in [a,b,c]} \frac{1}{d_i}}, p_A\right)), \quad (5)$$

where p_A represents the coordinates of point ‘A’.

After obtaining the feature maps at different resolutions, we perform feature propagation from coarse-grained feature maps to fine-grained feature maps. As shown in the right part of Figure 6, for a point ‘A’ in the dense point cloud, we find its k nearest points in the sparser point cloud. Then a lightweight DGCNN [60] is used to update the feature of ‘A’. We hierarchically update the feature with the resolution increases and finally obtain the dense feature map, which can be used for segmentation tasks. The detailed architecture for the segmentation head is shown in Table 6.